Abstracta

Ano XVI - N. 02

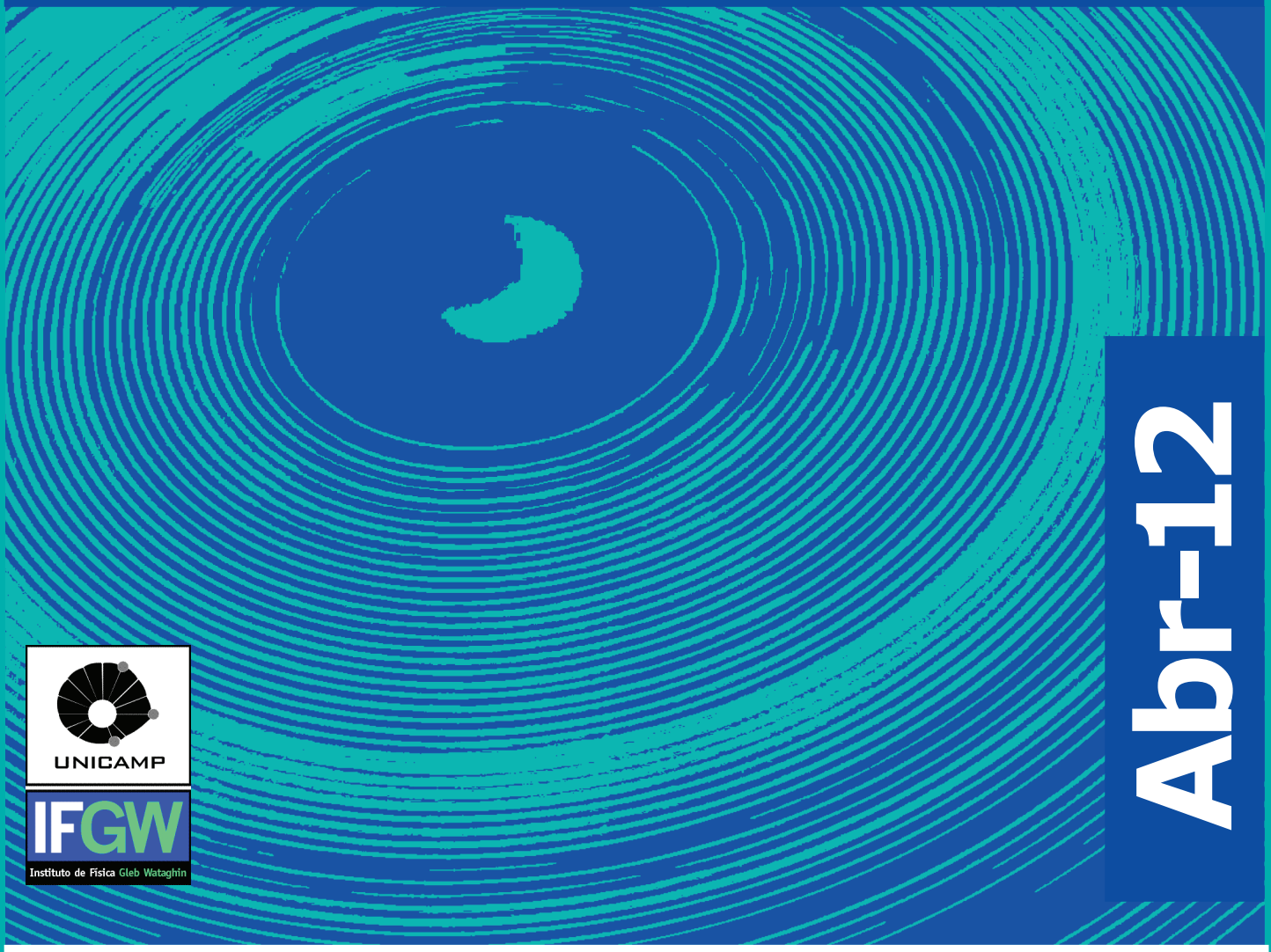

Abr-12

UNICAMP

IFGW

Instituto de Física Gleb Wataghin

Trabalhos Publicados

Janeiro à Abril 2012

P039-12 à P075-12

Trabalhos Aceitos para Publicação

A001-12

Capítulo de livro

Trabalhos Publicados

[P039-12] "A Novel Plasma Technique for Surface Treatment: The Plasma Expander"

Rangel, E. C.; Machida, M.; Durrant, S. F.; Cruz, N. C.

This paper describes a new plasma treatment method: the plasma expander. In this approach, expanding shock waves are generated in a vacuum chamber by pulsed plasmas. Collisions of fast species in the waves modify the properties of solid surfaces exposed to the plasma. The degree of such modification is governed by the energy delivered by the plasma exposure. To confirm the efficacy of this approach, modifications induced in the properties of thin polymer films produced by plasma-enhanced chemical vapor deposition by exposure to nitrogen plasma shock waves were investigated. The films were prepared from benzene radio frequency plasmas and subsequently exposed to different quantities of nitrogen shock waves N-w. The effects of N-w on the wettability, molecular structure, and mechanical properties of the films were studied. Fourier transform infrared spectroscopy revealed that greater N-w resulted in the loss of C-H groups and the rupture of benzene aromatic rings observed in the structure of the as-deposited films. Furthermore, the contact angle strongly increased and the hardness, evaluated by nanoindentation, increased up to fourfold with the increase in the intensity of the treatment.

IEEE Transactions on Plasma Science 40[2], 492-496, Part 2, 2012

[P040-12] "Broadband dispersion compensation using inner cladding modes in photonic crystal fibers"

Beltran-Mejia, F.; Cordeiro, C. M. B.; Andres, P.; Silvestre, E.

A photonic crystal fiber is optimized for chromatic dispersion compensation by using inner cladding modes. To this end, a photonic-oriented version of the downhill-simplex algorithm is employed. The numerical results show a dispersion profile that accurately compensates the targeted dispersion curve, as well as its dispersion slope. The presented fiber has a simple structure, while radiation losses can be reduced simply by adding a few more air-hole rings. Fabrication tolerances are also considered showing how fabrication inaccuracies effects can be overridden by just adjusting the compensation length.

Optics Express 20[4], 3467-3472, 2012

[P041-12] "Combination of electromagnetic physics processes for microdosimetry in liquid water with the Geant4 Monte Carlo simulation toolkit"

Ivanchenko, V. N.; Incerti, S.; Francis, Z.; Tran, H. N.; Karamitros, M.; Bernal, M. A.; Champion, C.; Gueye, P.

The Geant4 Monte Carlo simulation toolkit provides a set of electromagnetic physics processes adapted to the detailed simulation of particle interactions in liquid water for microdosimetry applications, such as single-cell irradiation with light ion beams. These processes, developed within the framework of the Geant4-DNA project, adopt a software design allowing their combination with other electromagnetic physics processes available in the Geant4 toolkit. This work describes the combination of Geant4-DNA electron processes with Geant4 photon processes.

Nuclear Instruments & Methods in Physics Research Section B-Beam Interactions With Materials and Atoms 273, 95-97, 2012

[P042-12] "Distribution of Counterions around Lignosulfonate Macromolecules in Different Polar Solvent Mixtures"

Vainio, U.; Lauten, R. A.; Haas, S.; Svedstrom, K.; Veiga, L. S. I.; Hoell, A.; Serimaa, R.

Lignosulfonate is a colloidal polyelectrolyte that is obtained as a side product in sulfite pulping. In this work we wanted to study the noncovalent association of the colloids in different solvents, as well as to find out how the charged sulfonate groups are organized on the colloid surface. We studied sodium and rubidium lignosulfonate in water-methanol mixtures and in dimethyl formamide. The number average molecular weights of the Na- and Rb-lignosulfonate fractions were 7600 g/mol and 9100 g/mol, respectively, and the polydispersity index for both was 2. Anomalous small-angle X-ray scattering (ASAXS) was used for determining the distribution of counterions around the Rb-lignosulfonate macromolecules. The scattering curves were fitted with a model constructed from ellipsoids of revolution of different sizes. Counterions were taken into account by deriving an approximative formula for the scattering intensity of the Poisson-Boltzmann diffuse double layer model. The interaction term between the spheroidal particles was estimated using the local monodisperse approximation and the improved Hayter-Penfold structure factor given by the rescaled mean spherical approximation. Effective charge of the polyelectrolyte and the local dielectric constant of the solvent close to the globular polyelectrolyte were followed as a function of the methanol content in the solvent and lignosulfonate concentration. The lignosulfonate macromolecules were found to aggregate noncovalently in water-methanol mixtures with increasing methanol or lignosulfonate content in a specific directional manner. The flat macromolecule aggregates had a nearly constant thickness of 1-1.4 nm, while their diameter grew when counterion association onto the polyelectrolyte increased. These results indicate that the charged groups in lignosulfonate are mostly at the flat surfaces of the colloid, allowing the associated lignosulfonate complexes to grow further at the edges of the complex.

Langmuir 28[5], 2465-2475, 2012

[P043-12] "Dynamics near a liquid-liquid phase transition in a non-tetrahedral liquid: The case of gallium"

Cajahuaringa, S.; de Koning, M.; Antonelli, A.

We use molecular simulation to analyze liquid dynamics in the vicinity of the liquid-liquid phase transition (LLPT) recently discovered in the modified embedded-atom model for elemental gallium. For this purpose we analyze the diffusive behavior in terms of the mean-squared displacement and self-intermediate scattering functions for two systems obtained by cooling the stable liquid through the LLPT at different cooling rates. The results show a pronounced heterogeneity of the dynamics upon the onset of the LLPT. Furthermore, it is found that this heterogeneity is closely correlated to the structural properties of the 9-fold coordinated high-density and 8-fold coordinated low-density liquid forms involved in the transition, showing a mixture of domains with very different diffusion time scales. The dynamics of the low-density liquid is found to be much more sluggish than that of the high-density form. Analysis of the energetics suggests that the origin of this difference is rooted in the fact that the cohesion in the former is significantly stronger than that in the latter.

Journal of Chemical Physics 136[6], 064513, 2012

[P044-12] "Effect of zinc concentration on the magnetic properties of cobalt-zinc nanoferrite"

Rani, R.; Sharma, S. K.; Pirota, K. R.; Knobel, M.; Thakur, S.; Singh, M.

Nano-cobalt zinc ferrite (CZFO) Co(1-x)ZnxFe2O4 with varied quantities of zinc (x = 0.0, 0.1, 0.2, 0.3, 0.4) have been prepared by solution combustion method. X-ray diffraction and transmission electron microscopy confirmed the size, structure and morphology of the nanoferrites. The addition of zinc in cobalt ferrite has been shown to play a crucial role in enhancing the magnetic properties. Ferromagnetic ordering is observed in nano samples at room temperature. Zn substitution shows maximum saturation magnetization for x = 0.1, that is 56.74 emu/g and then decreases for further increase in Zn substitution. The dependence of Mossbauer parameters viz. isomer shift and hyperfine magnetic field with zinc concentration has been studied. Mossbauer results are also supported by magnetization data. The results obtained from this method make these samples suitable for preparing high quality nanocrystalline ferrite for high density data storage applications.

Ceramics International 38[3], 2389-2394, 2012

[P045-12] "Element-specific and bulk magnetism, electronic, and crystal structures of La0.70Ca0.30Mn1-xCrxO3"

Terashita, H.; Cezar, J. C.; Ardito, F. M.; Bufaical, L. F.; Granado, E.

The magnetic interactions in La0.70Ca0.30Mn1-xCrxO3 (x = 0.15, 0.50, and 0.70) are investigated by x-ray absorption spectroscopy (XAS), x-ray magnetic circular dichroism (XMCD), high-resolution x-ray powder diffraction, and bulk magnetization measurements. XAS in the Mn and Cr L-2,L-3 edges support stable single valent Cr3+ ions and a varying Mn valence state with x, while the O K edge XAS spectrum reveals local maxima in the O 2p density of states close to the Fermi level due to mixing with Mn and Cr 3d states. A robust antiferromagnetic state is found for x = 0.70 below T-N = 258 K. For x = 0.15, combined XMCD and bulk magnetization measurements indicate a fully polarized ferrimagnetic state for the Mn and Cr spins below T-c = 224 K. For x = 0.50, a reduced ferrimagnetic component dominated by Mn spins is present below T-c = 154 K. No evidence of lattice anomalies due to cooperative charge and orbital orderings is found by x-ray diffraction for all samples. The magnetic properties of this system are rationalized in terms of a competition of ferromagnetic Mn-Mn double exchange and antiferromagnetic Cr-Cr and Cr-Mn superexchange interactions.

Physical Review B 85[10], 104401, 2012

[P046-12] "Energy dispersive X-ray reflectivity applied to the study of thermal stability of self-assembled organic multilayers: Results on phosphonic acids"

de Pauli, M.; Perez, C. A.; Prado, M. C.; Araujo, D. H. C.; Neves, B. R. A.; Malachias, A.

The temperature evolution of self-assembled phosphonic acid multilayers was investigated by energy dispersive X-ray reflectivity and angular-resolved reflectivity. Energy dispersive measurements were performed in an experimental setup specially designed for the X-ray fluorescence beamline of the Brazilian Synchrotron Light Laboratory. It allows the precise monitoring of phase transitions observed in organic thin film and multilayer systems. The studied multilayers - obtained from dip coating of a solution of octadecylphosphonic acid - present different bilayer periodicities of 50 angstrom (straight bilayer) and 34 angstrom (tilted bilayer). Energy dispersive and angular-resolved data evidence re-organization of the lamellar ordering of octadecylphosphonic acid multilayers as a function of temperature. The energy dispersive technique presents many advantages over conventional methods such as short acquisition time, possibility to vary external parameters and high flux, making it suitable for light scatterers as polymers and other organic molecules.

Synthetic Metals 161[23-24], 2521-2525, 2012

[P047-12] "Evaluation of the mean energy deposit during the impact of charged particles on liquid water"

Bernal, M. A.

The DNA strand break yield due to the impact of ionizing particles on living beings is closely related to the number of inelastic events per unit absorbed dose produced by these particles. The higher this number, the higher the probability of causing DNA strand breaks per unit absorbed dose. In a previous work, it was found that the total number of events produced by primary particles and the secondary electrons is almost independent of the type and energy of the incident particle (or LET). This finding could be supported by a quasi-constant mean energy deposit by inelastic event ((epsilon) over bar). In this work, (epsilon) over bar was defined and determined for electrons and the non-negative charge states of hydrogen (H-0,(+)) and helium (He-0,(+), (2+)) species impacting on liquid water. Ionization, excitation and charge transfer (up to two-electron transfers) processes have been included in present calculations. We found that, for liquid water, (epsilon) over bar is within 13.7 +/- 4.1 eV, 14.2 +/- 1.7 eV and 13.8 +/- 1.4 eV for electrons, hydrogen and helium species, respectively, with impact energies changing over three orders of magnitude. Unlike the mean excitation energy, the mean energy deposit per inelastic event depends not only on the target molecule but also on the projectile features. However, this dependence is relatively weak. This fact supports the quasi-independent number of inelastic events per unit absorbed dose found previously when charged particles impact on matter.

Physics in Medicine and Biology 57[7], 1745-1757, 2012

[P048-12] "Field profiles of bulk plasmon polariton modes in layered systems containing a metamaterial"

Bruno-Alfonso, A.; Reyes-Gomez, E.; Cavalcanti, S. B.; Oliveira, L. E.

Electric and magnetic fields in a one-dimensional layered system that alternates air and a metamaterial are investigated. Special attention is devoted to frequencies of electric and magnetic bulk plasmons. It is shown that plasmon polaritons nearby such frequencies display field profiles concentrated in the metamaterial, where the field component parallel to the stacking direction is essentially uniform and dominates the perpendicular one.

Journal of Physics-condensed Matter 24[4], 045302, 2012

[P049-12] "Harmonic decomposition of two particle angular correlations in Pb-Pb collisions at root s(NN)=2.76 TeV"

Aamodt, K.; Abelev, B.; Quintana, A. A.; Adamova, D.; Adare, A. M.; Aggarwal, M. M.; Rinella, G. A.; Agocs, A. G.; Agostinelli, A.; Salazar, S. A.; Ahammed, Z.; Ahmad, N.; Masoodi, A. A.; Ahn, S. U.; Akindinov, A.; Aleksandrov, D.; Alessandro, B.; Molina, R. A.; Alici, A.; et all.

Angular correlations between unidentified charged trigger (t) and associated (a) particles are measured by the ALICE experiment in Pb-Pb collisions at root s(NN) = 2.76 TeV for transverse momenta $0.25 < p(T)(t,a) < 15$ GeV/c, where $p(T)(t) > p(T)(a)$. The shapes of the pair correlation distributions are studied in a variety of collision centrality classes between 0 and 50% of the total hadronic cross section for particles in the pseudorapidity interval $|eta| < 1.0$. Distributions in relative azimuth Delta phi equivalent to phi(t) - phi(a) are analyzed for |Delta eta| equivalent to |eta(t) - eta(a)| > 0.8, and are referred to as "long-range correlations". Fourier components V-n Delta equivalent to < cos(n Delta phi)> are extracted from the long-range azimuthal correlation functions.

This suggests that no pair correlation harmonic can be described over the full 0.25 < p(T) < 15 GeV/c range using a single v(n) (p(T)) curve: such a description is however approximately possible for 2 <= n <= 5 when p(T)(a) < 4 GeV/c. For the n = 1 harmonic, however, a single v(1)(p(T)) curve is not obtained even within the reduced range p(T)(a) < 4 GeV/c. If particle pairs are correlated to one another through their individual correlation to a common symmetry plane, then the pair anisotropy V-n Delta (p(T)(t), p(T)(a)) is fully described in terms of single-particle anisotropies v(n)(p(T)) as V-n Delta(p(T)(t), p(T)(a)) = v(n)(p(T)(t))v(n)(p(T)(a)). This expectation is tested for 1 <= n <= 5 by applying a global fit of all V-n Delta(p(T)(t), p(T)(a)) to obtain the best values v(n){GF}(p(T)). It is found that for 2 <= n <= 5, the fit agrees well with data up to p(T)(a) similar to 3-4 GeV/c, with a trend of increasing deviation as p(T)(t) and p(T)(a) are increased or as collisions become more peripheral.

Physics Letters B 708[3-5], 249-264, 2012

[P050-12] "Heavy flavour decay muon production at forward rapidity in proton-proton collisions at root s=7 TeV"

Abelev, B.; Adam, J.; Adamova, D.; Adare, A. M.; Aggarwal, M. M.; Rinella, G. A.; Agocs, A. G.; Agostinelli, A.; Salazar, S. A.; Ahammed, Z.; Ahmad, N.; Masoodi, A. A.; Ahn, S. U.; Akindinov, A.; Aleksandrov, D.; Alessandro, B.; Molina, R. A.; Alici, A.; Alkin, A.; et all.

The production of muons from heavy flavour decays is measured at forward rapidity in proton-proton collisions at root s = 7 TeV collected with the ALICE experiment at the LHC. The analysis is carried out on a data sample corresponding to an integrated luminosity L-int = 16.5 nb(-1). The transverse momentum and rapidity differential production cross sections of muons from heavy flavour decays are measured in the rapidity range 2.5 < y <4, over the transverse momentum range 2 < p(t) < 12 GeV/c. The results are compared to predictions based on perturbative QCD calculations.

Physics Letters B 708[3-5], 265-275, 2012

[P051-12] "Identified Hadron Compositions in p plus p and Au plus Au Collisions at High Transverse Momenta at root s(NN)=200 GeV"

Agakishiev, G.; Aggarwal, M. M.; Ahammed, Z.; Alakhverdyants, A. V.; de Souza, R. D.; Takahashi, J.; Vasconcelos, G. M. S.; et all. STAR Collaboration

We report transverse momentum (p(T) <= 15 GeV/c) spectra of pi(+/-), K-+/-, p, (p) over bar, K-0(S), and rho(0) at midrapidity in p + p and Au + Au collisions at root s(NN) = 200 GeV. Perturbative QCD calculations are consistent with pi(+/-) spectra in p + p collisions but do not reproduce K and p((p) over bar) spectra. The observed decreasing antiparticle-to-particle ratios with increasing p(T) provide experimental evidence for varying quark and gluon jet contributions to high-p(T) hadron yields. The relative hadron abundances in Au + Au at p(T) >= 8 GeV/c are measured to be similar to the p + p results, despite the expected Casimir effect for parton energy loss.

Physical Review Letters 108[6], 072302, 2012

[P052-12] "Indication of Reactor (nu)over-bar(e) Disappearance in the Double Chooz Experiment"

Abe, Y.; Aberle, C.; Akiri, T.; dos Anjos, J. C.; Ardellier, F.; Barbosa, A. F.; Baxter, A.; Bergevin, M.; Bernstein, A.; Bezerra, T. J. C.; Bezrukhov, L.; Blucher, E.; Bongrand, M.; Bowden, N. S.; Buck, C.; Busenitz, J.; Cabrera, A.; Caden, E.; Camilleri, L.; Carr, R.; Cerrada, M.; Chang, P. J.; et all.

The Double Chooz experiment presents an indication of reactor electron antineutrino disappearance consistent with neutrino oscillations. An observed-to-predicted ratio of events of 0.944 +/- 0.016(stat) +/- 0.040(syst) was obtained in 101 days of running at the Chooz nuclear power plant in France, with two 4.25 GW(th) reactors. The results were obtained from a single 10 m(3) fiducial volume detector located 1050 m from the two reactor cores. The reactor antineutrino flux prediction used the Bugey4 flux measurement after correction for differences in core composition. The deficit can be interpreted as an indication of a nonzero value of the still unmeasured neutrino mixing parameter sin(2)2 theta(13). Analyzing both the rate of the prompt positrons and their energy spectrum, we find sin(2)2 theta(13) 0.086 +/- 0.041(stat) +/- 0.030(syst), or, at 90% C.L., 0.017 < sin(2)2 theta(13) < 0.16.

Physical Review Letters 108[13], 131801, 2012

[P053-12] "Investigating thermal properties of biodiesel/diesel mixtures using photopyroelectric technique"

Guimaraes, A. O.; Machado, F. A. L.; da Silva, E. C.; Mansanares, A. M.

In this work we explored the photopyroelectric technique (PPE) for the thermal characterization of biodiesel/diesel and other binary liquid mixtures, such as ethanol and ethylene glycol in water. We have used the back configuration (BPPE), in the thickness scan approach, and the front one (FPPE), in the frequency scan approach, for getting the thermal diffusivity and effusivity values, respectively. For all the measured systems, we got good data fittings when using the model proposed by Matvienko and Mandelis for thermal diffusivity of liquid mixtures. In addition, we could evidence the different strength in the molecular interaction related to the several mixtures, based on the normalized excess values for thermal diffusivity, as proposed by Dadarlat et al. For biodiesel/diesel mixtures, which present weak cohesive interactions among the saturated/aromatic hydrocarbons of diesel and the alkyl esters of biodiesel, we proposed a semi empirical model for the thermal diffusivity, based on the logarithm mixing model for the thermal conductivity and a simple addictive law for the heat capacity per unit volume.

Thermochimica Acta 527, 125-130, 2012

[P054-12] "Isotope effects in high-T-c cuprate superconductors as support for the bipolaron theory of superconductivity"

Alexandrov, A. S.; Zhao, G. M.

We provide a unified parameter-free explanation of the observed oxygen-isotope effects on the critical temperature, the magnetic-field penetration depth and on the normal-state pseudogap for underdoped cuprate superconductors within the framework of the multi-(bi)polaron theory with strong Coulomb and Frohlich interactions. We also quantitatively explain the measured critical temperature and the magnitude of the magnetic-field penetration depth. This paper thus represents an important support for the bipolaron theory of high-temperature superconductivity, compatible with many other independent observations.

New Journal of Physics 14, 013046, 2012

[P055-12] "J/psi Polarization in pp Collisions at root s=7 TeV"

Abelev, B.; Quintana, A. A.; Adamova, D.; Adare, A. M.; Chinellato, D. D.; Cosentino, M. R.; Dash, A.; Takahashi, J.; et all. ALICE Collaboration

The ALICE Collaboration has studied J/psi production in pp collisions at root s = 7 TeV at the LHC through its muon pair decay. The polar and azimuthal angle distributions of the decay muons were measured, and results on the J/psi polarization parameters lambda(theta) and lambda(phi) were obtained. The study was performed in the kinematic region 2: 5 < y < 4, 2 < p(t) < 8 GeV/c, in the helicity and Collins-Soper reference frames. In both frames, the polarization parameters are compatible with zero, within uncertainties.

Physical Review Letters 108[8], 082001, 2012

[P056-12] "Locally inaccessible information as a fundamental ingredient to quantum information"

Fanchini, F. F.; Castelano, L. K.; Cornelio, M. F.; de Oliveira, M. C.

Quantum discord (QD) measures the fraction of the pairwise mutual information that is locally inaccessible in a multipartite system. Fundamental aspects related to two important measures in quantum information theory, namely the entanglement of formation (EOF) and the conditional entropy, can be understood in terms of the distribution of this form of local inaccessible information (LII). As such, the EOF for an arbitrarily mixed bipartite system AB can be related to the gain or loss of LII due to the extra knowledge that a purifying ancillary system E has on the pair AB. Similarly, a clear meaning of the negativity of the conditional entropy for AB is given. We employ these relations to elucidate important and yet not well-understood quantum features, such as the bipartite entanglement sudden death and the distinction between EOF and QD for quantifying quantum correlation. For that we introduce the concept of LII flow that quantifies the LII shared in a multipartite system when sequential local measurements are carried out.

New Journal of Physics 14, 013027, 2012

[P057-12] "Low energy spin dynamics in the spin ice Ho2Sn2O7"

Ehlers, G.; Huq, A.; Diallo, S. O.; Adriano, C.; Rule, K. C.; Cornelius, A. L.; Fouquet, P.; Pagliuso, P. G.; Gardner, J. S.

The magnetic properties of Ho2Sn2O7 have been investigated and compared to other spin ice compounds. Although the lattice has expanded by 3% relative to the better studied Ho2Ti2O7 spin ice, no significant changes were observed in the high temperature properties, T greater than or similar to 20 K. As the temperature is lowered and correlations develop, Ho2Sn2O7 enters its quantum phase at a slightly higher temperature than Ho2Ti2O7 and is more antiferromagnetic in character. Below 80 K a weak inelastic mode associated with the holmium nuclear spin system has been measured. The hyperfine field at the holmium nucleus was found to be approximate to 700 T.

Journal of Physics-Condensed Matter 24[7], 076005, 2012

[P058-12] "Magneto-optical investigation of two-dimensional gases in n-type resonant tunneling diodes"

Galeti, H. V. A.; Gobato, Y. G.; Gordo, V. O.; dos Santos, L. F.; Brasil, M. J. S. P.; Lopez-Richard, V.; Marques, G. E.; Orlita, M.; Kunc, J.; Maude, D. K.; Henini, M.; Airey, R. J.

We have studied the polarized emission from the contact layers and the quantum well of asymmetric n-type GaAs/GaAlAs resonant tunneling diodes under high magnetic fields (up to 19 T) parallel to the tunnel current. The photoluminescence from the GaAs contact layers shows evidence of the recombination from a two-dimensional hole gas accumulated next to the GaAlAs barrier and free carriers. Both the energy position and the intensity of this emission are voltage dependent. In addition, the photoluminescence from the two-dimensional hole gas and quantum well is strongly spin-polarized under the applied voltage and high magnetic fields. Pronounced oscillatory features are observed in the magnetic field dependence of the polarization degree from the quantum well and the two-dimensional hole emissions at integer filling factors. The obtained data show that resonant tunneling diodes are interesting systems to study the physical properties of voltage-controlled two-dimensional gases in the accumulation layers and quantum well.

Semiconductor Science and Technology 27[1], 015018, 2012

[P059-12] "Measurement of charm production at central rapidity in proton-proton collisions at root s=7 TeV"

Abelev, B.; Quintana, A. A.; Adamova, D.; Adare, A. M.; Aggarwal, M. M.; Rinella, G. A.; Agocs, A. G.; Agostinelli, A.; Salazar, S. A.; Ahammed, Z.; Ahmad, N.; Masoodi, A. A.; Ahn, S. U.; Akindinov, A.; Aleksandrov, D.; Alessandro, B.; Molina, R. A.; Alici, A.; et all.

The p(t)-differential inclusive production cross sections of the prompt charmed mesons D-0, D+, and D*(+) in the rapidity range vertical bar y vertical bar < 0.5 were measured in proton-proton collisions at root s = 7 TeV at the LHC using the ALICE detector. Reconstructing the decays D-0 -> K-pi(+), D+ -> K-pi(+) pi(+), D*(+) -> D-0 pi(+), and their charge conjugates, about 8,400 D-0, 2,900 D+, and 2,600 D*(+) mesons with 1 < p(t) < 24 GeV/c were counted, after selection cuts, in a data sample of 3.14 x 10(8) events collected with a minimum-bias trigger (integrated luminosity L-int = 5 nb(-1)). The results are described within uncertainties by predictions based on perturbative QCD.

Journal of High Energy Physics [1], 128, 2012

[P060-12] "Nonstandard Neutrinos Interactions in a 331 Model with Minimum Higgs Sector"

Medina, M.; de Holanda, P. C.

We present a detailed analysis of a class of extensions to the SM Gauge chiral symmetry SU(3)(C) x SU(3)(L) x U(1)(x) (331 model), where the neutrino electroweak interaction with matter via charged and neutral current is modified through new gauge bosons of the model. We found the connections between the nonstandard contributions on 331 model with nonstandard interactions. Through limits of such interactions in cross-section experiments, we constrained the parameters of the model, obtaining that the new energy scale of this theory should obey V > 1.3 TeV and the new bosons of the model must have masses greater than 610 GeV.

Advances in High Energy Physics, 763829, 2012

[P061-12] "Novel Sealing Technique for Practical Liquid-Core Photonic Crystal Fibers"

Gerosa, R. M.; Bozolan, A.; de Matos, C. J. S.; Romero, M. A.; Cordeiro, C. M. B.

In this letter, we describe a simple and effective technique to prevent evaporation in liquid-core photonic crystal fibers (PCFs). The technique consists of using a micropipette to deploy a micro-droplet of an ultraviolet curable polymer adhesive in both core inputs. After it is cured, the adhesive creates sealing polymer plugs with quite satisfactory insertion loss (overall optical transmission of about 15%). Processed fibers remained liquid-filled for at least six weeks. From a practical point of view, we conducted a supercontinuum generation experiment in a water-core PCF to demonstrate a 120-minute spectral width stability and the ability to withstand at least 3-mW average power at the sealed fiber input. Similar experiments carried out with nonsealed fibers produced supercontinuum spectra lasting no longer than 10 minutes, with average powers kept below 0.5 mW to avoid thermally induced evaporation.

IEEE Photonics Technology Letters 24[3], 191-193, 2012

[P062-12] "Particle-Yield Modification in Jetlike Azimuthal Dihadron Correlations in Pb-Pb Collisions at root S-NN=2.76 TeV"

Aamodt, K.; Abelev, B.; Quintana, A. A.; Adamova, D.; Adare, A. M.; Chinellato, D. D.; Cosentino, M. R.; Dash, A.; Takahashi, J.; et all. ALICE Collaboration

The yield of charged particles associated with high-pt trigger particles (8 < p(t) < 15 GeV/c) is measured with the ALICE detector in Pb-Pb collisions at root S-NN = 2.76 TeV relative to proton-proton collisions at the same energy. The conditional per-trigger yields are extracted from the narrow jetlike correlation peaks in azimuthal dihadron correlations. In the 5% most central collisions, we observe that the yield of associated charged particles with transverse momenta p(t) > 3 GeV/c on the away side drops to about 60% of that observed in pp collisions, while on the near side a moderate enhancement of 20%-30% is found.

Physical Review Letters 108[9], 092301, 2012

[P063-12] "Photothermally modulated magnetic resonance applied to the study of the magnetic phase transition in gadolinium thin films"

Soffner, M. E.; Tedesco, J. C. G.; Pedrochi, F.; Gadioli, G. Z.; de Moraes, M. A. B.; Guimaraes, A. O.; da Silva, E. C.; Mansanares, A. M.

We explore the photothermally modulated magnetic resonance technique to investigate gadolinium thin films deposited on fused quartz substrate, as a function of thickness and thermal treatment, around the magnetic phase transition temperature. It has been observed that the maximum amplitude of the photothermally modulated magnetic resonance (PM-MR) signal takes place near the phase transition temperature, similarly to the magnetocaloric effect, for which Gd has been the prototype material. The reason is that both depend on the temperature derivative of the magnetization, which maximizes at the phase transition. Besides, there is a narrowing of transition with thermal treatment, confirming that thermal treatment stabilizes the film structure. For frequency scan measurements, the heat diffusion in a two-layer system was considered, and a depth profile study was carried out in order to investigate heterogeneities along the film thickness. From the PM-MR response as a function of the modulation frequency it was possible to estimate the thermal properties of the Gd film. Magnetization, X-ray and electron spin resonance measurements were used to complement the analysis and support the conclusions.

Thin Solid Films 520[9], 3634-3640, 2012

[P064-12] "Physical properties of nanofluid suspension of ferromagnetic graphite with high Zeta potential"

Souza, N. S.; Rodrigues, A. D.; Cardoso, C. A.; Pardo, H.; Faccio, R.; Mombru, A. W.; Galzerani, J. C.; de Lima, O. F.; Sergeenkov, S.; Araujo-Moreira, F. M.

We report on the magnetic properties and stability of nanofluid ferromagnetic graphite (NFMG) studied through the measurements of its magnetization hysteresis curves. Raman spectrum and the so-called Zeta potential. The obtained results suggest a robust ferromagnetic behavior of NFMG even at room temperature along with a good stability of the dispersed solution (with Zeta potential around 41.3 mV) and a good reactivity between magnetic graphite and CTAB type cationic surfactant.

Physics Letters A 376[4], 544-546, 2012

[P065-12] "Physico-chemical properties of Brazilian cocoa butter and industrial blends. Part II - Microstructure, polymorphic behavior and crystallization characteristics"

Ribeiro, A. P. B.; Basso, R. C.; Goncalves, L. A. G.; Gioielli, L. A.; dos Santos, A. O.; Cardoso, L. P.; Kieckbusch, T. G.

The microstructural behavior of industrial standardized cocoa butter samples and cocoa butter samples from three different Brazilian states is compared. The cocoa butters were characterized by their microstructural patterns, crystallization kinetics and polymorphic habits. The evaluation of these parameters aided in establishing relationships between the chemical compositions and crystallization behavior of the samples, as well as differentiating them in terms of technological and industrial potential for use in tropical regions.

Grasas y Aceites 63[1], 89-99, 2012

[P066-12] "Purification of metallurgical silicon by horizontal zone melting"

Mei, P. R.; Moreira, S. P.; Cardoso, E.; Cortes, A. D. S.; Marques, F. C.

In this study, we aimed at systematically determining the potential of the zone melting (ZM) technique to remove impurities from Metallurgical Grade Silicon (MG- Si) in an Electron Beam Furnace (EBF), using a water-cooled copper crucible. Our focus was on obtaining solar grade silicon, with the purity between Electronic Grade Silicon (EG-Si) and MG-Si, at lower cost than the silicon obtained by the Siemens process. The MG- Si (99.855% purity in mass, or 1,450 ppm of impurities) was processed by 1 and 2 passes of ZM at speed of 1 mm/min and 10 mm/min. The ZM process reduced in 98% the total amount of impurities present in the MG-Si, increasing the purity from 99% to 99.999%, an intermediate stage to achieve the electronic grade (> 99.9999%). Boron remained near the same after the ZM due to its vapor pressure be lower than the pressure of the furnace chamber and due its distribution coefficient in silicon be near the unit. Carbon and oxygen in the MG-Si were reduced from 106 to 35 ppm and from 30 ppm to 5 ppm, respectively, after ZM, and these values are very close to the levels in the electronic grade silicon. The electrical resistivity showed to be dependent on the boron concentration, but not on the phosphorus or the total amount of impurities. All ingots processed by ZM exhibited p-type characteristics, and it means that boron was really the dominant dopant.

Solar Energy Materials and Solar Cells 98, 233-239, 2012

[P067-12] "Quantum magnetic oscillations and angle-resolved photoemission from impurity bands in cuprate superconductors"

Alexandrov, A. S.

Present-day angle-resolved photoemission spectroscopy (ARPES) has offered a tremendous advance in the understanding of electron energy spectra in cuprate superconductors and some related compounds. However, in high magnetic field, magnetic quantum oscillations at low temperatures indicate the existence of small electron (hole) Fermi pockets seemingly missing in ARPES of hole (electron) doped cuprates. Here ARPES and quantum oscillations are reconciled in the framework of an impurity band in the charge-transfer Mott-Hubbard insulator.

Physical Review B 85[9], 2012

[P068-12] "rho(0) photoproduction in AuAu collisions at root s(NN)=62.4 GeV measured with the STAR detector"

Agakishiev, G.; Aggarwal, M. M.; Ahammed, Z.; Alakhverdyants, A. V.; de Souza, R. D.; Takahashi, J.; Vasconcelos, G. M. S. Star Collaboration

Vector mesons may be photoproduced in relativistic heavy-ion collisions when a virtual photon emitted by one nucleus scatters from the other nucleus, emerging as a vector meson. The STAR Collaboration has previously presented measurements of coherent rho(0) photoproduction at center of mass energies of 130 GeV and 200 GeV in AuAu collisions. Here, we present a measurement of the cross section at 62.4 GeV; we find that the cross section for coherent rho(0) photoproduction with nuclear breakup is 10.5 +/- 1.5 +/- 1.6mb at 62.4 GeV. The cross-section ratio between 200 GeV and 62.4 GeV is 4.4 +/- 0.6, less than is predicted by most theoretical models. It is, however, proportionally much larger than the previously observed 15% +/- 55% increase between 130 GeV and 200 GeV.

Physical Review C 85[1], 014910, 2012

[P069-12] "Search for Lorentz invariance and CPT violation with muon antineutrinos in the MINOS Near Detector"

Adamson, P.; Ayres, D. S.; Barr, G.; Bishai, M.; Coelho, J. A. B.; Escobar, C. O. MINOS Collaboration

We have searched for sidereal variations in the rate of antineutrino interactions in the MINOS Near Detector. Using antineutrinos produced by the NuMI beam, we find no statistically significant sidereal modulation in the rate. When this result is placed in the context of the Standard Model Extension theory we are able to place upper limits on the coefficients defining the theory. These limits are used in combination with the results from an earlier analysis of MINOS neutrino data to further constrain the coefficients.

Physical Review D 85[3], 031101, 2012

[P070-12] "Search for signatures of magnetically-induced alignment in the arrival directions measured by the Pierre Auger Observatory"

Abreu, P.; Aglietta, M.; Ahn, E. J.; Albuquerque, I. F. M.; Allard, D.; Allekotte, I.; Allen, J.; Allison, P.; Castillo, J. A.; Alvarez-Muniz, J.; Ambrosio, M.; Aminaei, A.; Anchordoqui, L.; Andringa, S.; Anticic, T.; Anzalone, A.; Aramo, C.; Arganda, E.; Arqueros, F.; et all.

We present the results of an analysis of data recorded at the Pierre Auger Observatory in which we search for groups of directionally-aligned events (or 'multiplets') which exhibit a correlation between arrival direction and the inverse of the energy. These signatures are expected from sets of events coming from the same source after having been deflected by intervening coherent magnetic fields. The observation of several events from the same source would open the possibility to accurately reconstruct the position of the source and also measure the integral of the component of the magnetic field orthogonal to the trajectory of the cosmic rays. We describe the largest multiplets found and compute the probability that they appeared by chance from an isotropic distribution. We find no statistically significant evidence for the presence of multiplets arising from magnetic deflections in the present data.

Astroparticle Physics 35[6], 354-361, 2012

[P071-12] "Strangeness Enhancement in Cu-Cu and Au-Au Collisions at root s(NN)=200 GeV"

Agakishiev, G.; Aggarwal, M. M.; Ahammed, Z.; Alakhverdyants, A. V.; de Souza, R. D.; Takahashi, J.; Vasconcelos, G. M. S.; et all. Star Collaboration

We report new STAR measurements of midrapidity yields for the Lambda, (Lambda) over bar, K-S(0), Xi(-), (Xi) over bar (+), Omega(-), (Omega) over bar (+) particles in Cu + Cu collisions at root s(NN) = 200 GeV, and midrapidity yields for the Lambda, (Lambda) over bar, K-S(0) particles in Au + Au at root s(NN) = 200 GeV. We show that, at a given number of participating nucleons, the production of strange hadrons is higher in Cu + Cu collisions than in Au + Au collisions at the same center-of-mass energy. We find that aspects of the enhancement factors for all particles can be described by a parametrization based on the fraction of participants that undergo multiple collisions.

Physical Review Letters 108[6], 072301, 2012

[P072-12] "Structural and photophysical properties of anthracenyl and carbazolyl groups in silicone-based polymers"

Domingues, R. A.; Martins, T. D.; Yoshida, I. V. P.; Brasil, M. J. S. P.; Atvars, T. D. Z.

This paper describes a simple methodology to attach luminescent groups (anthracenyl and carbazolyl) to polysiloxanes (silicone), using hydrosilylation reactions between the Si-H groups from the silicone precursor to vinyl derivatives of the lumophores. The photophysical properties of these luminescent silicones were studied using both steady-state and dynamical photoluminescence spectroscopy. A strong correlation was obtained between the structural characteristics of the anthracenyl- and carbazolyl-based polysiloxanes, depending on the amount and the position of the Si-H bonds in the silicone precursors. For sparsely distributed Si-H groups, both the anthracenyl-labeled and carbazolyl-labeled polysiloxanes showed photophysical properties (fluorescence spectrum and fluorescence decays) similar to those of 1-alkyl anthracenyl and 1-alkyl carbazolyl derivatives, respectively. Nevertheless, for closely spaced Si-H groups, emission and decay are different. The presence of excimers was observed for anthracenyl but not for carbazolyl polysiloxanes. This latter observation is quite different from that observed for carbon-based polymers for which the carbazolyl excimer formation is a very common process probably due to the differences in the silicone structure.

Journal of Luminescence 132[4], 972-978, 2012

[P073-12] "Superlight small bipolarons from realistic long-range Coulomb and Frohlich interactions"

Alexandrov, A. S.; Samson, J. H.; Sica, G.

We report analytical and numerical results on the two-particle states of the polaronic t-J(p) model derived recently with realistic Coulomb and electron-phonon (Frohlich) interactions in doped polar insulators. Eigenstates and eigenvalues are calculated for two different geometries. Our results show that the ground state is a bipolaronic singlet, made up of two polarons. The bipolaron size increases with increasing ratio of the polaron hopping integral t to the exchange interaction J(p) but remains small in the whole range 0 <= t/Jp <= 1. Furthermore, the model exhibits a phase transition to a superconducting state with a critical temperature well in excess of 100 K since the small bipolarons are perfectly mobile. In the range t/Jp <= 1, there are distinct charge and spin gaps opening in the density of states, specific heat, and magnetic susceptibility well above T-c.

Physical Review B 85[10], 2012

[P074-12] "Terahertz Photometer to Observe Solar Flares in Continuum"

Marcon, R.; Kaufmann, P.; Fernandes, L. O. T.; Godoy, R.; Marun, A.; Bortolucci, E. C.; Zakia, M. B.; Diniz, J. A.; Kudaka, A. S.

Solar observations at sub-THz frequencies detected a new flare spectral component peaking in the THz range, simultaneously with the well known microwaves component, bringing challenging constraints for interpretation.

Higher THz frequencies observations are needed to understand the nature of the mechanisms occurring in flares. A THz photometer system was developed to observe outside the terrestrial atmosphere on stratospheric balloons or satellites, or at exceptionally transparent ground stations. The telescope was designed to observe the whole solar disk detecting small relative changes in input temperature caused by flares at localized positions. A Golay cell detector is preceded by low-pass filters to suppress visible and near IR radiation, a band-pass filter, and a chopper. A prototype was assembled to demonstrate the new concept and the system performance. It can detect temperature variations smaller than 1 K for data sampled at a rate of 10/s, smoothed for intervals larger than 4 s. For a 76 mm aperture, this corresponds to small solar burst intensities at THz frequencies. A system with 3 and 7 THz photometers is being built for solar flare observations on board of stratospheric balloon missions.

Journal of Infrared Millimeter and Terahertz Waves 33[2], 192-205, 2012

[P075-12] "The influence of magnetic and electric coupling properties on the magnetocaloric effect in quantum paraelectric EuTiO(3)"

von Ranke, P. J.; Alho, B. P.; Nobrega, E. P.; de Sousa, V. S. R.; Alvarenga, T. S. T.; Carvalho, A. M. G.; de Oliveira, N. A.

We report on the magnetic and magnetocaloric effect calculations in antiferromagnetic perovskite-type EuTiO(3). From the isothermal magnetic entropy change calculated upon low magnetic field changes (below 1 T) several results were predicted: inverse magnetocaloric effect, latent heat associated to spin AFM-FM reorientation transition and a temperature interval (controlled by magnetic field) where the EuTiO(3) does not change heat in an isothermic process. The magnetocaloric effect described through magnetic entropy change was correlated with magnetocapacitance formula. The theoretical investigation was carried out using a Heisenberg Hamiltonian considering the G-type antiferromagnetic structure with exchange interactions, in mean field approximation, between nearest-neighbor and next-nearest-neighbor magnetic Eu(+2) ions.

Journal of Magnetism and Magnetic Materials 324[7], 1290-1295, 2012

Trabalhos Aceitos para Publicação

[A001-12] "Structural, optical and electrical properties of indium nitride polycrystalline films"

da Silva, M. V. S.; David, D. G. F.; Pepe, I.; da Silva, A. F.; de Almeida, J. S.; Gazoto, A. L.; dos Santos, A. O.; Cardoso, L. P.; Meneses, E. A.; Graybill, D. L.; Mertes, K. M.

The structural, optical and electrical properties of InN polycrystalline films on glass substrate are investigated by means of X-ray photoelectron spectroscopy, Raman scattering measurements, X-ray diffraction analysis, optical spectroscopy, and electrical measurements as a function of the inverse of temperature. The absorption edge for the films is most likely due to an impurity band formed by the presence of defects in the material. Such an impurity band, located at 1.6 eV extends itself to about 1.8 eV above the Fermi level, and it is attributed to nitrogen vacancies present in the material. The Raman scattering data also reveal the incorporation of oxygen in the InN films, leading to the formation of the In2O3 amorphous phase during the process of sputtering. Additionally, the X-ray photoelectron spectroscopy of the valence band, which is highly desirable to the determination of the Fermi level, confirms the optical gap energy. Furthermore, the X-ray diffraction patterns of the thinner films present broader peaks, indicating high values for the strain between the film lattice and the glass substrate. Finally, first principles calculations are used to investigate the optical properties of InN and also to support the experimental findings.

Thin Solid Films, Aceito em 04 de março de 2012

Capítulo de livro

"Ion-Beam-Induced Epitaxial Method and Its Recent Applications Recrystallization."

LANG, Rossano; MENEZES, Alan de; SANTOS, Adenilson dos; REBOH, Shay; MENESES, Eliermes; AMARAL, Livio; CARDOSO, Lisandro

In: SZTWIERTNIA, Krzysztof (Org.). Recrystallization. [s.l.]: Intech, 2012. Cap. 14, p. 351-370. Disponível em: <http://www.intechopen.com/books/recrystallization/ion-beam-induced-epitaxial-recrystallization-method-and-its-recent-applications>. Open Access.

Abstracta

Instituto de Física
Diretor: Prof. Dr. Daniel Pereira
Universidade Estadual de Campinas - UNICAMP
Cidade Universitária Zeferino Vaz
13083-859 - Campinas - SP - Brasil
e-mail: secdir@ifi.unicamp.br
Fone: 0XX 19 3521-5300

Publicação

Biblioteca do Instituto de Física Gleb Wataghin
http://webbif.ifi.unicamp.br
Diretora Técnica: Sandra Maria Carlos Cartaxo

Elaboração
Maria Graciele Trevisan
graciele@ifi.unicamp.br

Projeto Gráfico
ÍgneaDesign

Impressão

Gráfica Central - Unicamp